Efficient *p*-type doping of sputter-deposited NiO thin films with Li, Ag, and Cu acceptors

Kingsley O. Egbo,[1] Chinedu E. Ekuma,[2,*] Chao Ping Liu,[1,3] and Kin Man Yu[1,4,†]

[1]*Department of Physics, City University of Hong Kong, 83 Tat Chee Avenue, Kowloon, Hong Kong*
[2]*Department of Physics, Lehigh University, Bethlehem, Pennsylvania 18015, USA*
[3]*Research Center for Advanced Optics and Photoelectronics, Department of Physics, College of Science, Shantou University, Shantou, Guangdong 515063, China*
[4]*Department of Material Science and Engineering, City University of Hong Kong, 83 Tat Chee Avenue, Kowloon, Hong Kong*

(Received 15 June 2020; accepted 24 September 2020; published 20 October 2020)

Nickel oxide, NiO, is an important *p*-type oxide semiconductor that has been studied for applications in solar cells, junction diodes, and other optoelectronic devices. In a nominally undoped NiO, depending on its oxygen stoichiometry, it only has a modest *p*-type conductivity of ∼0.1 S/cm due to Ni vacancy acceptors. However, the overall transport can be improved by extrinsic doping. In this study, we carry out a combined experiment and computational study of the effects of acceptor dopants, including Li, Ag, and Cu on the properties of NiO. Our *ab initio* calculations show that among all the acceptors studied, substitutional Li (Li_{Ni}) acceptor species has the lowest formation and ionization energies. Measured electrical properties of the undoped and doped oxygen-rich NiO ($NiO_{1+\delta}$) show an increase in conductivity and hole concentration for the doped samples. In particular, Li is an efficient acceptor to achieve highly conducting *p*-type NiO with >40% transmittance in the visible range for a 100-nm-thick film. The improvement in the electrical properties with different dopant species studied is in good agreement with the calculated defect formation and ionization energies. A remarkable increase in the temperature-dependent Hall mobility is also observed in the doped samples. Based on the small-polaron hoping model, we analyzed the conduction mechanism in the doped samples, which revealed a hopping dominated activation with energies in the range of 172–208 meV.

DOI: 10.1103/PhysRevMaterials.4.104603

I. INTRODUCTION

The development of *p*-type materials that combine high optical transparency with excellent electrical properties is of great technological interest [1]. Wide band-gap transition metal (TM) oxides constitute an important class of materials that have been explored for applications as transparent conductors (TCs) [2,3]. However, most TM oxides have the proclivity to be *n*-type, and *p*-type doping of these oxides is difficult, if not impossible. This can be attributed to the mostly O 2*p* character of the valence band states in TM oxides; and this makes the development of TM oxide-based *p*-type TCs with comparable properties as their *n*-type counterparts such as In_2O_3, SnO_2, and ZnO challenging [4,5]. A notable exception is NiO, which is one of the few *p*-type TM oxides. Moreover, NiO also has a wide direct energy band gap of approximately 3.4–4.1 eV; making it useful for a broad range of electronic and optoelectronic device applications such as ultraviolet photodetectors, heterojunction diodes, electrochromic devices, and as hole transport layers in perovskite and organic solar cells [6–10].

Nominally undoped NiO is insulating but becomes *p*-type conducting when grown in oxygen-rich conditions, primarily due to the presence of Ni vacancies (V_{Ni}) which have a relatively low formation energy [11,12]. In contrast, the compensating donor defects or "hole killers," such as oxygen vacancies, V_O, and Ni interstitials, Ni_i are much less likely to form due to their higher formation energies [11]. However, the *p*-type conductivity in O-rich NiO due to native acceptors is limited and unstable. Intentional doping of NiO by acceptor impurities to increase the free hole density and achieve better, stable *p*-type conductivity has been explored. In recent decades, a lot of work has been carried out to improve the conductivity of NiO with substitutional dopants such as Li [13], Cs [14], Cu [15], Co [16], and Al [17].

In general, the formation energy of extrinsic dopant defects in a semiconductor gives insights on the dopant solubility, while its ionization energy determines the free carrier concentration at room temperature. Furthermore, as the dopant concentration increases, the formation of compensating native defects may become energetically favorable, and hence limit the doping efficiency. Therefore, for efficient *p*-type doping in NiO with high dopant concentration, the acceptor dopant must have low formation energy and relatively low ionization energy. At the same time, formation energies of compensating native donor defects (such as Ni interstitials Ni_i and O vacancies V_O) have to be high [18].

Developing a highly conducting *p*-type NiO requires an understanding of the nature and interaction of these extrinsic dopants with the host atoms and various native defects present in the material. Hence, it is necessary to establish a detailed understanding of the effects of acceptor dopants on the

*che218@lehigh.edu
†kinmanyu@cityu.edu.hk

 ©2020 American Physical Society

optoelectronic properties of NiO. In this study, we combine experimental work with *ab initio* calculations to explore the changes in the electrical and optical properties of NiO doped with several acceptor species, namely, Li, Cu, and Ag. We synthesized NiO thin films with different concentrations of Li, Cu, and Ag dopants by the radio frequency (RF) magnetron sputtering method using pure argon and a mixture of $Ar + O_2$ as the sputtering gas to obtain "stoichiometric" (NiO) and O-rich materials ($NiO_{1+\delta}$), respectively. We performed detailed characterization of the influence of various dopants on optical and transport properties of the deposited samples. The transport properties were further studied using temperature dependent Hall measurements and analyzed with the Arrhenius conduction and the hopping conduction models. Experimental results are correlated with calculated defect formation energies and transition levels of the various dopant species. Comparisons of measured core level x-ray photoelectron and valence band spectra with the calculated total and projected density of states provided further insights on the influence of the dopants on the electronic structure of NiO thin films. Our experimental and calculated results show that although Cu and Ag can be used to improve the *p*-type conductivity of $NiO_{1+\delta}$, Li is the most efficient acceptor to achieve a highly conducting and transparent *p*-type $NiO_{1+\delta}$.

II. EXPERIMENTAL AND COMPUTATIONAL DETAILS

A. Experiments

Doped and undoped NiO and O-rich NiO ($NiO_{1+\delta}$) thin-film samples were deposited at room temperature on glass substrates using a multigun radio-frequency (RF) magnetron sputtering system. The oxygen flow ratio, $r(O_2) = f(O_2)/[f(\mathrm{Ar}) + f(O_2)]$ in the sputtering gas was controlled by flowing pure Ar and O_2 during deposition. All O-rich samples were grown in an O-rich environment with a $r(O_2) =$ 1.4%. Cu and Ag doping were achieved by co-sputtering NiO with Cu and Ag metal targets, respectively using a DC power source. Films with desired Cu and Ag dopant composition were obtained by varying the sputtering power of the metal and NiO targets. Li doping was achieved by using a Li doped NiO ceramic target (with 9% Li), and films with Li composition lower than 9% was achieved by co-sputtering with a NiO target.

Film stoichiometry and thickness were measured by Rutherford backscattering (RBS) using a 3.04-MeV He^{++} beam. Film thicknesses in the range of 80–120 nm were determined by RBS. Grazing incidence x-ray diffraction (GIXRD) with a grazing incidence angle of 1° was used to characterize the film structure. All the films were polycrystalline with an average grain size of ∼16 nm, as revealed from the diffraction peak widths. Rocksalt (111) and (200) diffraction peaks are observed in XRD patterns from all samples. Electrical properties of doped and undoped $NiO_{1+\delta}$ thin films were investigated by variable-temperature (200–500 K) Hall effect measurements in the *van der Pauw* geometry with a magnetic field of 0.54 T using a commercial (Ecopia HMS-5300) system. Room temperature thermopower measurements were obtained using an MMR SB1000 thermopower system. Optical properties of doped and undoped NiO films were studied by UV-Vis-NIR spectrophotometry and standard spectroscopic ellipsometry (SE) between the spectral range of 0.74–6.5 eV. In the SE measurement, the ellipsometry parameters, amplitude ratio, Ψ and phase difference, Δ spectra were recorded at incident angles of 55°, 65°, and 75°. The real and imaginary parts of the complex dielectric function were obtained by fitting the Ψ and Δ spectra from all the angles of incidence using a model with Tauc-Lorentz oscillators. The surface roughness was accounted for via the Bruggeman effective medium approximation [19]. The dielectric function of the glass substrate used has been described previously [20]. The core levels and valence band spectra were probed by high-resolution x-ray photoelectron spectroscopy (XPS) using a monochromatic Al K_α x-ray source. Collected photoelectrons were analyzed using a concentric hemispherical analyzer system. Electrostatic charging effects for insulating samples were corrected by monitoring the binding energy of the C 1*s* photoemission signal from surface hydrocarbon contaminants.

B. Computational approach

Our calculations were based on first-principles density functional theory [21,22]. We used the Perdew-Burke-Ernzerhof exchange-correlation functional [23] and the projector augmented-wave basis set as implemented in the Vienna *ab initio* simulation package (VASP) [24]. To account for electron-electron interactions and exchange coupling interactions of the valence *d* states, we used the Hubbard potential *U* and the exchange interaction *J* (DFT + *U*). We adopt a *U* value of 5.10 eV for Ni, which is smaller than the typical value of ∼7–8 eV used for NiO. This choice of *U* is motivated by previous works that show smaller *U* values better describes the experimental optical properties [25]. For Cu, we used a *U* value of ∼7.0 eV from a previous study [26], and a *J* value of 0.95 eV is adopted for the respective atoms. We note that a different choice of *U* value for Cu-*d* states has a negligible impact on the electronic and optical properties because the contribution of the Cu-*d* state to the states in the proximity of the Fermi level is very small. The unit cell of NiO is rocksalt with a rhombohedral symmetry due to the type-II antiferromagnetic order along the [111] direction. For the defect calculations, we used a 108-atom rhombohedral supercell and doping concentration of 3.70%, for effective comparison to ∼4.0% doping concentration data in the experiment. All the structures were relaxed with a Γ-point sample of the reciprocal space, allowing all the atomic positions and cell volume to relax until the energy (charge) is converged to within $\sim 10^{-3}$ eV (10^{-6} eV) and the forces dropped to 10^{-3} eV/Å. The self-consistency calculations used a $3\times3\times3$ *k*-point grid to represent the reciprocal space. They were performed in the antiferromagnetic phase maintaining the type-II antiferromagnetic order of NiO using a collinear spin-polarized approach with a kinetic energy cutoff of 550 eV for the plane-wave basis set. The electronic structures were used to obtain the optical properties based on the linear response function.

The formation energy $E^f(X, q)$ of a defect *X* in charge state *q* in our calculation is described by

$$E^f(X, q) = E_{\mathrm{tot}}(X, q) - E_{\mathrm{tot}}(\mathrm{bulk}) - \sum_i n_i \mu_i + qE_F + E_{\mathrm{corr}}, \quad (1)$$

where $E_{tot}(X, q)$ is the total energy associated with each charged/neutral defect in NiO, E_{tot}(bulk) is the total energy of the pristine NiO, E_F is the energy of the Fermi level, n_i is the number of atoms of type i (host atom or impurity atom) that have been removed from ($n_i < 0$) or added to ($n_i > 0$) the perfect crystal to form the defect, μ_i is the chemical potential associated with elemental species, i referenced to the total energy per atom of the respective standard phase, and E_{corr} is the sum of all the needed correction energy, including a correction term due to the presence of periodic images that becomes necessary for charged defects in the supercell calculations [27]. Charge transition level $\epsilon(q_1/q_2)$ defined as the Fermi level values for which two charge states q_1 and q_2 have equal defect formation energies is obtained as

$$(q_1/q_2)\frac{E^f(X, q_1; E_F = 0) - E^f(X, q_2; E_F = 0)}{q_2 - q_1}, \quad (2)$$

where $E^f(X, q; E_F = 0)$ is the formation energy of the defect X in the charge state q when the Fermi level is at the valence band maximum (VBM) ($E_F = 0$). The position of the transition level is an indication of how shallow or deep a charged defect state is with reference to the valence band maximum (VBM).

In our calculations, integral quantities such as the local magnetic moments at the Ni sites are used to obtain the degree of localization in the system. However, due to the local reorganization, some of the typically nonmagnetic systems acquire small but finite magnetic moments, leading to enhanced magnetic behavior. The obtained local magnetic moments, m in μ_B for the antiferromagnetic NiO is 1.62 μ_B. The computed value agrees closely with values obtained previously by Rödl *et al.* [28] but underestimates the experimental local magnetic moments in NiO, which has a value of 1.90 μ_B [29]. The dopants in NiO led to negligible changes in the magnetic moment of NiO. The calculated local magnetic moments of Li, Cu, and Ag doped NiO are 1.61 μ_B, 1.62 μ_B, and 1.68 μ_B, respectively. In the defect structures, the O atom acquired a small but finite magnetic moment of ±0.02 μ_B. We predict the magnetic moment of Li in NiO:Li to be $-0.04\,\mu_B$ while that of Ag in NiO:Ag is obtained to be 0.18 μ_B. The magnetic moment of Cu in NiO:Cu is predicted to be 0.62 μ_B, very close to $\sim$0.68 μ_B reported by experiment and computation for Cu in CuO [26,30,31].

III. RESULTS AND DISCUSSION

A. Optical properties

The real (ε_1) and imaginary (ε_2) parts of the complex dielectric functions [$\varepsilon(\omega) = \varepsilon_1(\omega) + i\varepsilon_2(\omega)$] of our 4% doped thin films obtained by SE fittings are presented in Figs. 1(a) and 1(c), respectively, while the calculated spectra are shown in Figs. 1(b) and 1(d). Note that these samples were grown in pure Ar environment ("stoichiometric" NiO films); hence no intentional Ni vacancies are introduced. Only slight changes in the ε_1 and ε_2 spectra of these deposited films are observed with doping. These experimental $\varepsilon_1(\omega)$ and $\varepsilon_2(\omega)$ spectra agree reasonably well with the calculated data for energies $>$1 eV. Doping induced variations in both ε_1 and ε_2 are more evident across the photon energies in the calculated spectra. Calculated ε_1 spectra [Fig. 1(b)] of all the doped samples show a decrease in the peak amplitude at $\sim$3 eV. Compared to the undoped NiO, the calculated ε_1 of the NiO:Li and NiO:Ag shows a marked decrease below 2 eV. Since the absorption coefficient α is related to ε_2, the onsets of ε_2 at $\sim$3 eV for all samples indicate transitions between the VBM and the conduction minimum (CBM). The calculated ε_2 spectra in Fig. 1(d) shows that above this fundamental absorption edge, ε_2 rises to an asymmetrical peak at $\sim$3.6 eV (E_1). A decrease in the amplitude of this characteristic E_1 peak at $\sim$3.6 is also observed for the doped samples. Notably, in the calculated results, ε_2 of doped NiO differs substantially from that of the undoped NiO for energies $<$2 eV. Among the doped samples, the ε_2 spectra of NiO:Cu show the least changes but with a small local maximum at $\sim$1.5 eV. The ε_2 spectra of the NiO:Ag show a gradual increase below 2 eV with a local maximum at $\sim$0.6 eV. For the NiO:Li, the ε_2 spectra show similar behavior as the Ag-doped sample except that a local maximum is not observable but it exhibits a strong increase for photon energy $<$0.5 eV.

Absorption coefficients of the undoped and doped NiO obtained from the calculated dielectric functions are shown in Fig. 2(a). The computed spectra show that the incorporation of any of three dopants leads to increased sub-gap absorption of NiO, especially for energies $<$2 eV. The magnitude of these defect-induced sub-gap absorptions below 3 eV is different for different dopants with their local maximum at $\sim$0.5, 0.8, and 1.5 eV for Li, Ag, and Cu dopants, respectively. In Fig. 2(b), the experimental absorption coefficient spectra extracted from the SE data for the samples grown in Ar and O-rich conditions are compared. Note that for the "stoichiometric" samples, the calculated spectra in Fig. 2(a) exhibit more features at higher photon energies compared to the experimental spectra in Fig. 2(b), likely due to the small broadening parameter $\sim10^{-3}$ used in our calculations. The crystallinity and the grain size of the polycrystalline films may also broaden these features in the experimental data. In the experimental absorption coefficient spectra shown in Fig. 2(b), only slight increase in subgap absorption are observed for NiO films with doping while the local maxima present in the calculated spectra are not detected in the experimental data.

From Fig. 2(b), the experimental absorption coefficient of the O-rich thin films ($NiO_{1+\delta}$) (dashed lines) shows substantial increase in subgap absorptions for energies $<$3 eV which is attributed to Ni vacancy defects. The calculated absorption coefficient of an undoped NiO with V_{Ni} in Fig. 2(a) illustrates the strong effect of these native defects on the optical property of NiO in good agreement with the experimental absorption coefficients of the $NiO_{1+\delta}$ samples in Fig. 2(b). Note that both the experimental and calculated results show that the effects of V_{Ni} are dominant in the subgap absorption of both doped and undoped $NiO_{1+\delta}$ samples and the effects of dopants on the absorption become insignificant.

Values of the optical band gap extracted from our calculations are also compared with the experimental results as shown in Table I. The experimental results were obtained via the extrapolation of the $(\alpha h\nu)^2$ versus $h\nu$ plot of the absorption coefficient for the "stoichiometric" films grown without extra oxygen. Our experiments show that band gap of NiO decrease slightly when doped with the acceptors by

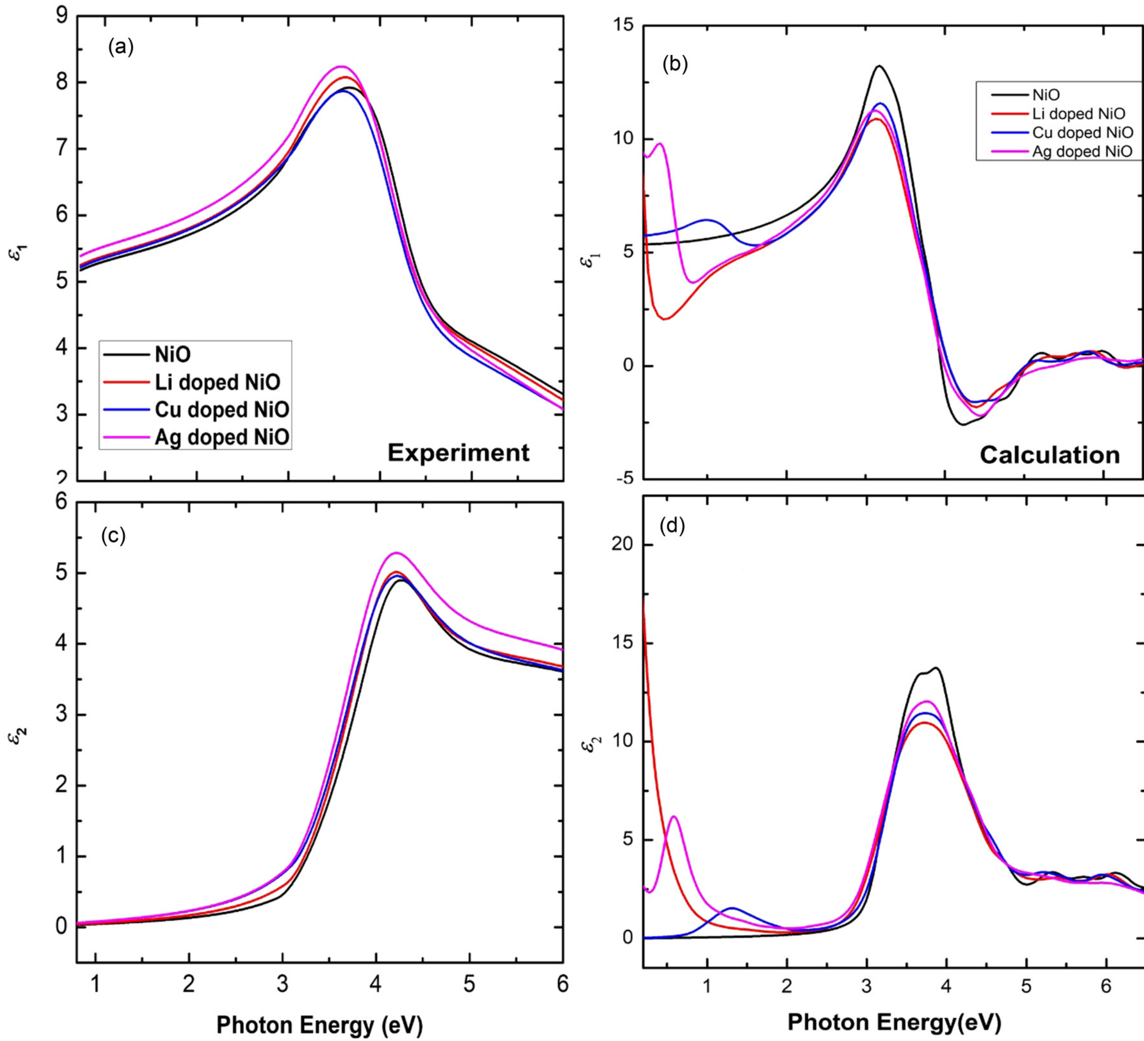

FIG. 1. Measured (a) real ε_1 and (c) imaginary ε_2 parts and calculated (b) real ε_1 and (d) imaginary ε_2 parts of the complex dielectric function of NiO and doped NiO systems.

$\sim$0.15–0.2 eV. A similar dopant induced band-gap reduction is also observed in the calculated results. Compared to the experimental results, band gaps obtained by our calculations are consistently lower by $\sim$0.3 eV.

It is well established that the presence of Ni vacancies, V_{Ni} in NiO grown in an O-rich condition results in *p*-type conductivity. The undoped and doped $\mathrm{NiO}_{1+\delta}$ films are *p*-type conducting and their electrical properties will be discussed in the next section. As shown in Fig. 2(b) the subgap absorption is significant in all these *p*-type conducting films, presumably arising from defect gap states. The high subgap absorption coefficient of these materials results in a strong reduction in the film transmittance. Figure 3 shows the transmission intensity for 100-nm-thick *p*-type undoped and doped $\mathrm{NiO}_{1+\delta}$ compared with that of a "stoichiometric" undoped NiO. Notice the strong reduction in the transmittance of the O-rich samples compared with the stoichiometric sample. While the transmittance of the $\mathrm{NiO}_{1+\delta}$:Li film is similar to the undoped $\mathrm{NiO}_{1+\delta}$, a slight reduction is observed for $\mathrm{NiO}_{1+\delta}$ films doped with Cu and Ag.

B. Electrical properties

In the electrical properties of the doped and undoped *p*-type $\mathrm{NiO}_{1+\delta}$, the hole generation mechanism can be described using the Kroger-Vink notation [32]. The primary native acceptors in $\mathrm{NiO}_{1+\delta}$ are Ni vacancies, V_{Ni} and/or O interstitials, O_i. They can contribute free holes ($\oplus$) when ionized [singly charged (V'_{Ni} and O'_i) or doubly charged (V''_{Ni} and O''_i)] according to the reactions

$$V_{\mathrm{Ni}} \rightleftharpoons V'_{Ni} + \oplus, \tag{3}$$

$$V'_{Ni} \rightleftharpoons V''_{Ni} + \oplus, \tag{4}$$

$$O_i \rightleftharpoons O'_i + \oplus, \tag{5}$$

$$O'_i \rightleftharpoons O''_i + \oplus. \tag{6}$$

With additional extrinsic doping with acceptor species $\boldsymbol{M}$ ($\boldsymbol{M}$ = Li, Cu, and Ag in this study), $\boldsymbol{M}$ can substitute Ni

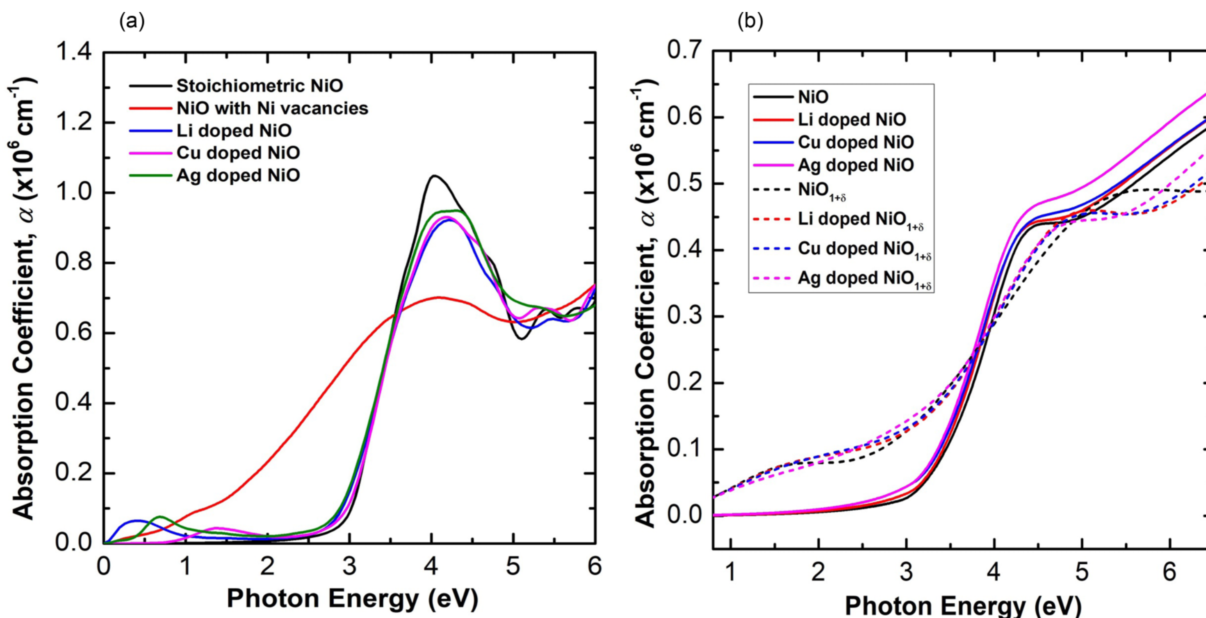

FIG. 2. (a) Calculated absorption spectra of stoichiometric NiO, NiO with Ni vacancies, and doped NiO. (b) Absorption spectra extracted from fittings of spectroscopic ellipsometry data for undoped and doped NiO (solid lines) and undoped and doped $NiO_{1+\delta}$ (dashed lines).

forming $\boldsymbol{M}_{\mathrm{Ni}}$ giving rise to free holes according to the reaction

$$\boldsymbol{M}_{\mathrm{Ni}} \rightleftharpoons \boldsymbol{M}'_{Ni} + \oplus. \quad (7)$$

Therefore it is expected that extrinsic doping with $\boldsymbol{M}$ acceptors will lead to an improvement in the *p*-type conductivity compared to undoped $NiO_{1+\delta}$ samples provided the $\boldsymbol{M}$ acceptors can reside on substitutional Ni site and form relatively shallow acceptor levels.

1. Hall effect measurements

Table II summarizes the room temperature (RT) resistivity, ρ of 4% doped and undoped $NiO_{1+\delta}$ thin films. The 4% doped samples were selected for the purpose of direct comparing the measured optical and electrical properties with the calculated optical properties and the formation and transition energies. In Table S1 [33], we further showed the changes in the electrical properties of the $NiO_{1+\delta}$ thin films with Li, Cu and Ag doping at different dopant concentration obtained from RT Hall effect measurements. Table II shows that the resistivity decreases with doping. Among the dopant species, Li leads to the highest decrease in the resistivity and achieves a $\rho(\mathrm{RT}) \sim 0.2\,\Omega\,\mathrm{cm}$. We note that the RT mobilities of NiO are rather low (on the order of $10^{-1}\,\mathrm{cm}^2\,\mathrm{V}^{-1}\,\mathrm{s}^{-1}$), and may not be accurately determined from our hall setup, this also makes the conductivity type ambiguous [34,35]. However, at temperatures above 380 K, as shown in Fig. 4, all samples exhibit reliable Hall mobilities $\sim\mu_h > 1.5\,\mathrm{cm}^2\,\mathrm{V}^{-1}\,\mathrm{s}^{-1}$, with only small variations in the hole concentration, p. Hence we can reasonably estimate the RT mobilities by using the RT resistivity and assuming that RT hole concentation is equal to the hole concentration at 380 K; $p(\mathrm{RT}) = p(380\,\mathrm{K})$ [36,37]. The results are tabulated in Table II. Moreover, room temperature thermopower measurements were performed, and all undoped and doped $NiO_{1+\delta}$ samples are confirmed to be *p*-type from their positive Seebeck coefficients, S as shown in

TABLE I. Calculated and experimental optical band gap of undoped and doped NiO.

	NiO	Li:NiO	Cu:NiO	Ag:NiO
Calculation	3.24	3.03	3.10	3.09
Experiment	3.60	3.45	3.42	3.40

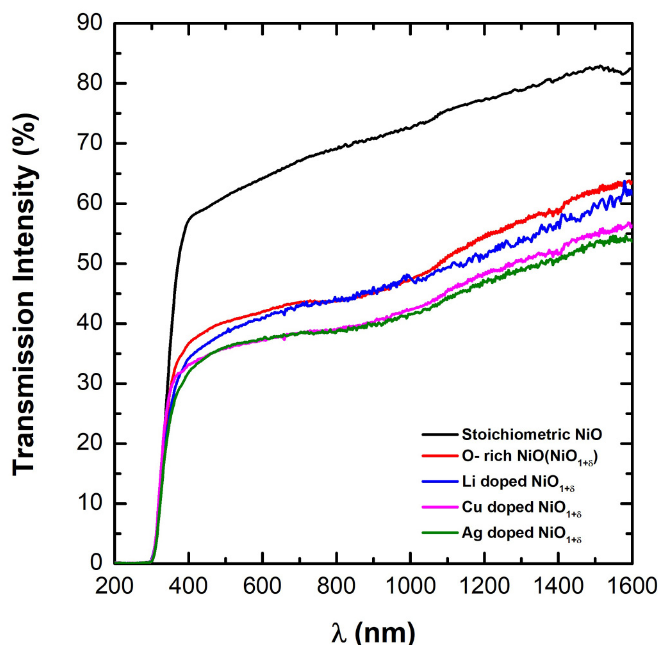

FIG. 3. Measured transmission intensity for the *p*-type undoped and doped O-rich $NiO_{1+\delta}$ thin films with thickness of 100 nm. Stoichiometric NiO transmission intensity spectrum is also shown for comparison.

TABLE II. RT measured resistivity, Seebeck coefficient, and estimated RT mobility values of 4% doped and undoped $NiO_{1+\delta}$.

Sample	ρ (Ω cm)	S (μV/K)	μ(cm^2 V^{-1} s^{-1})
Undoped $NiO_{1+\delta}$	2.85	+108	0.440
Li doped	0.20	+60	1.5
Cu doped	0.81	+83	0.97
Ag doped	0.24	+67	0.60

Table II. Comparing to the undoped sample ($S = 106\,\mu$V/K), values of S for the doped $NiO_{1+\delta}$ are lower by a factor of 25%–45% (in the range of 60–83 μV/K). Since the magnitude of S decreases with increasing carrier concentration [38], our results suggest that the doped $NiO_{1+\delta}$ films have higher hole concentration.

Electrical properties of the doped polycrystalline $NiO_{1+\delta}$ thin films in this study shown in Table II are comparable and in many cases much better than previously reported NiO thin films with equivalent doping levels deposited by similar physical vapor deposition methods. For instance, Dutta *et al.*, obtained a resistivity of 0.41 Ωcm for their ∼4% $Li_xNi_{1-x}O$ thin films [39], Zhang *et al.*, obtained a resistivity of 0.37 Ω cm and a mobility of 0.047 cm^2 V^{-1} s^{-1} for their 3% Li doped NiO thin films [40]. For a Li doping concentration of ∼6%, Jang *et al.*, reported an electrical resistivity of ∼0.39 Ω-cm [13]. A resistivity of 35.8 Ωcm was reported by Chen *et al.*, for ∼9% Cu doped NiO thin films [41]. Ishikawa *et al.*, showed a resistivity of ∼8.3 Ωcm for their ∼9% Ag doped thin film samples [42].

Figure 4 shows the temperature dependence of the resistivity ρ, hole concentration p, and hall mobility μ_h of 4% doped and undoped $NiO_{1+\delta}$. We observe that the Li doped $NiO_{1+\delta}$ sample exhibits the best electrical properties (highest μ and lowest ρ) compared to undoped and Cu- and Ag-doped samples. Moreover, all samples show the characteristic semiconductor behavior of decreasing resistivity with increasing temperature. Compared to the undoped sample, the p-type resistivity shows a remarkable decrease with doping. Li doped samples exhibit the lowest resistivity across measured temperature range followed by Ag-doped and Cu doped samples, respectively. Reliable hole concentration and Hall mobility for temperatures between 360–450 K are presented in Figs. 4(b) and 4(c), respectively. From Fig. 4(b), only a slight decrease in the hole concentration is observed for all samples with increasing temperature. In contrast, the increase in the mobility with temperature in various samples shown in Fig. 4(c) is more notable. The temperature dependence of μ_h of the Li doped sample is particularly strong. For example, μ_h increases from ∼5 cm^2 V^{-1} s^{-1} at 380 K to ∼15 cm^2 V^{-1} s^{-1} at 450 K.

2. Formation and transition energies of dopants

To understand the measured electrical properties of the various NiO samples, we also carried out *ab initio* calculations of the formation and transition energies of native as well as the dopant defects in $NiO_{1+\delta}$ and the results are presented in Table III. As shown in Table III, the transition levels of V_{Ni}, $\epsilon(0/-1) = E_V + 0.39$ eV is obtained. The calculated formation energy of the substitutional dopants $\boldsymbol{M}_{Ni}$ is lower than that of V_{Ni}. The lower formation energies of the dopants are expected to lead to a higher equilibrium solubility which in turn leads to an increase in the hole density. From our calculated data, among the dopants, Li_{Ni} has the lowest formation energy, followed by Cu and Ag dopants. Moreover, $E^f(Li_{Ni})$ has a negative value, suggesting that the formation of this defect is energetically favorable, and the solubility of Li in NiO is expected to be high.

In Table III, the charge transition levels $\epsilon(q_1/q_2)$ of the substitutional dopant defects are referenced to the valence band maximum. The hole concentration for doped samples showed only a slight temperature dependence, suggesting that shallow acceptors are prevalent. Among the dopant species studied, Li_{Ni} also has the shallowest transition level $\epsilon(0/-1)$ of +0.12 eV, and its hole concentration shows the least variation with temperature. A combination of low formation energy and small charge transition state enables Li dopant to be an efficient acceptor in NiO which can achieve highly p-type conducting $NiO_{1+\delta}$. Lany *et al.*, also reported similar low formation energies for Li dopants in NiO [11]. The calculated results in Table III also suggest that although Cu and Ag are not as efficient as Li as p-type dopant, Cu_{Ni} and Ag_{Ni} have relatively low formation energies leading to high solubility

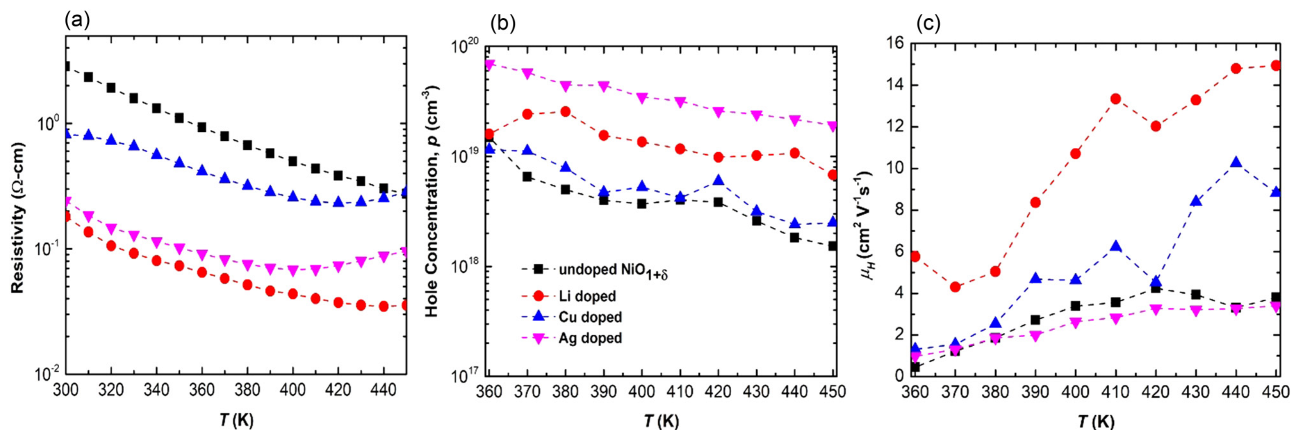

FIG. 4. Temperature dependence of (a) resistivity, (b) hole concentration, and (c) mobility of undoped and doped $NiO_{1+\delta}$ thin films.

TABLE III. Calculated formation energies and transition level for the electrically active dopant defects of 3.7% Li, Cu, and Ag and 3.7% Ni vacancies.

Defect	$E^f(q=0)$	$E^f(q=-1)$	$E^f(q=-2)$	$\epsilon(0/-1)$	$\epsilon(-1/-2)$
V_{Ni}	6.593	6.992	8.398	0.39	1.70
Li_{Ni}	−1.920	−1.792	–	0.12	–
Cu_{Ni}	2.021	2.051	2.413	0.3	1.18
Ag_{Ni}	4.451	4.817	4.812	0.36	0.99

in NiO and hence result in higher carrier concentration than undoped samples. This is in good agreement with our Hall measurements shown in Table II and Fig. 4.

3. Transport mechanism

In the variable-temperature data for both undoped and doped $NiO_{1+\delta}$, the increase in mobility at almost constant carrier concentration for temperatures above 360 K suggests a possible thermally activated hopping. To study the transport properties, we consider polaronic effects in these $NiO_{1+\delta}$ samples due to the low mobilities obtained from the Hall data at room temperature and the remarkable increase in mobility at high temperature. Small polaron hopping (SPH) conduction due to self-trapping of holes in *p*-type materials lead to unfavorable low mobilities described by the Bosman-van Daal limit [43–45]. The carrier self-trapping, which is a result of the localization of holes at a specific lattice location, forming a hole state leads to these low mobilities. This SPH mechanism and the variable range hopping have been used to successfully describe hole conduction in *p*-type NiO and other *p*-type metal oxide systems previously [11,37,38,43].

In the SPH model, the temperature and conductivity can be related according to the equation; $\sigma T = \sigma_0 T \exp(-E_{ah}/kT)$, where k is the Boltzmann constant, and E_{ah} is the hopping activation energy [40,46,47]. Plots of the measured temperature-dependent conductivity data for the various samples according to the SPH model, $\ln(\sigma T)$ versus $(1/T)$, are shown in Fig. 5(a). Reasonable linear fits can be obtained for all plots in the measured temperature range as shown with the dashed lines.

Table IV shows the hopping activation energies, E_{ah} for undoped, Cu-, Ag-, and Li-doped $NiO_{1+\delta}$ thin films. These results are close to the reported hopping activation energy for Li-doped NiO epitaxial thin films (0.166–0.224 eV) [40]. These hopping activation energies directly impact the nature of hole mobilities in this high-temperature range. From Table IV, we find that undoped and Ag-doped $NiO_{1+\delta}$ films have higher hopping activation energies, resulting in a much smaller increase in the mobility at elevated temperature, as shown in Fig. 4(c).

To further study whether the measured carrier activation is indeed limited by the hopping activation or acceptor activation, the temperature dependence of the acceptor activation energy using the Arrhenius plot is also analyzed and presented in Fig. 5(b). The Arrhenius activation energies, E_a are also shown in Table IV. The Arrhenius activation energies for all samples are smaller than the hopping activation energies, indicating that the conductivity in our system may be dominated by hopping conduction [47]. The obtained hopping activation energies for our system show that the thermal ionization for the hole bound small polarons are quite low compared to many oxide materials which require comparatively higher energies of ∼>0.5 eV [48].

C. Electronic structure and density of states

To explore the effects of these dopants and understand the electronic properties of doped NiO thin films, we compare their electronic structures obtained by high-resolution x-ray photoelectron spectroscopy (XPS) with the calculated density of states (DOS). From our calculated total density of states shown in Fig. S1 [33], we observed no significant changes when dopants are introduced in NiO. This is expected as the dopant concentration at 4% may not lead to significant changes in the electronic structure. However, slight distinctions are observed in the valence band maximum positions of the DOS for the doped systems compared to undoped NiO. In particular, the onset of the valence band maximum is closer to

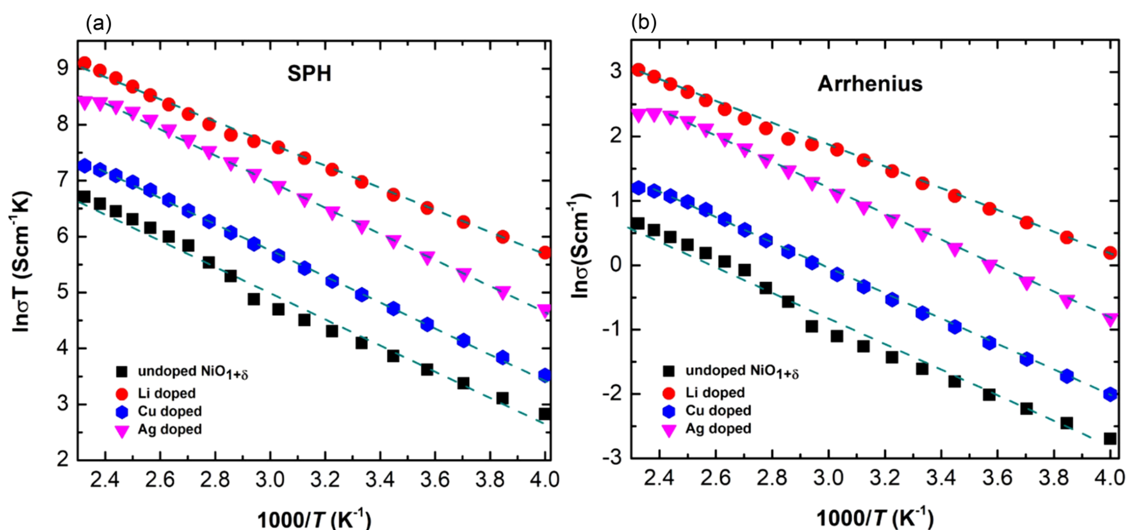

FIG. 5. Temperature-dependent conductivity plotted in (a) the small polaron hopping conduction model (b) Arrhenius conduction model.

TABLE IV. Hopping activation (SPH) and Arrhenius activation energies obtained from fitting the electrical data (Fig. 5).

Sample	SPH E_{ah}(eV)	Arrhenius E_a (eV)
Undoped $NiO_{1+\delta}$	0.208 ± 0.023	0.180 ± 0.021
Li doped	0.172 ± 0.015	0.144 ± 0.012
Cu doped	0.198 ± 0.007	0.170 ± 0.004
Ag doped	0.201 ± 0.009	0.172 ± 0.005

the Fermi energy at 0 eV for the Li doped NiO compared to the undoped NiO. This is attributed to the shallow Li acceptor states.

The XPS valence band spectra of doped and undoped NiO are shown in Fig. 6. Relative positions of the VBM (E_V) with respect to the Fermi level E_F ($E_F - E_V$) were obtained by convoluting a step function with a Gaussian function according to the procedure outlined previously [49]. An ($E_F - E_V$) value of ≈0.4 eV is obtained for undoped NiO thin film. With Cu and Ag doping, the E_F moves closer to E_V so that ($E_F - E_V$) ≈ 0.3 eV. A more dramatic decrease in ($E_F - E_V$) to ≈0.1 eV is observed for the Li doped NiO. The movement of the Fermi level closer to the valence band with doping is consistent with the increase in hole concentration and this is also in good agreement with the calculated DOS shown in Fig. S1 [33].

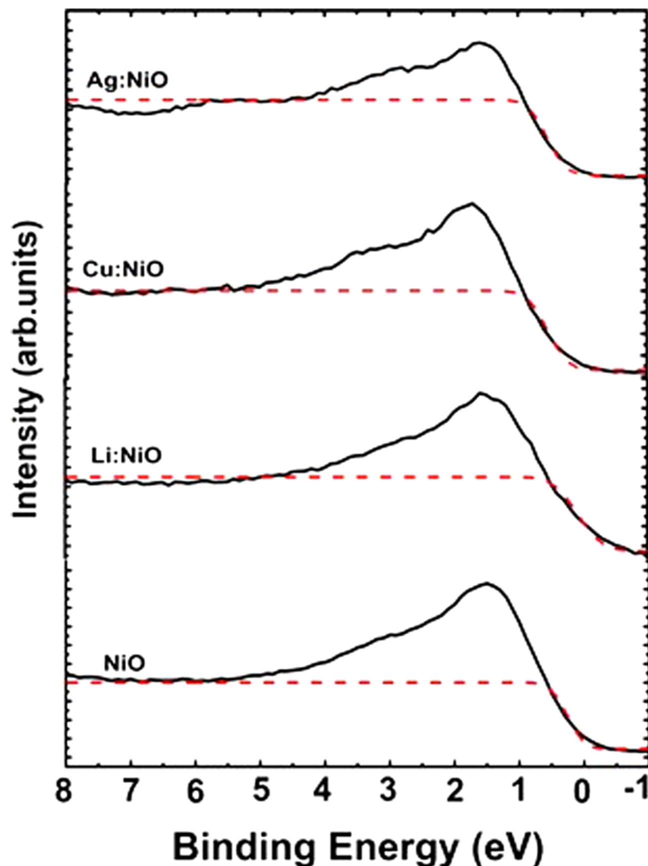

FIG. 6. XPS valence-band spectra of NiO and doped NiO. The dashed line spectra are fits to the XPS spectra with a step function convoluted with a Gaussian function used to determine the ($E_F - E_V$) value of the films.

IV. CONCLUSIONS

Achieving good hole mobility and conductivity is generally difficult in *p*-type TM binary oxides due to their high hole effective mass caused by the nature of the valence band. Among known *p*-type oxides, a high energy position of the valence band maximum in NiO facilitates its *p*-type dopability. In this work, we compared the effects of acceptor dopants on the optical and electrical properties as well as the electronic structures of NiO through a combination of experimental and computational approaches. Li-, Cu-, Ag-doped, and undoped polycrystalline NiO and O-rich NiO ($NiO_{1+\delta}$) were synthesized by RF magnetron sputtering. We demonstrate that the electrical properties of *p*-type $NiO_{1+\delta}$ can be improved by all the extrinsic acceptor dopants in this study. In particular, we find that the Li doped sample shows the most promising electrical properties followed by the Ag-doped samples, while Cu doping results in a relatively smaller improvement. The room temperature *p*-type conductivity of $NiO_{1+\delta}$ doped with Li, Ag, and Cu is 5.0, 4.16, and 1.23 S/cm, respectively while the undoped $NiO_{1+\delta}$ has a lower conductivity of 0.35 S/cm. Variable temperature mobility measurements indicate a thermally activated behavior in all the thin films and the carrier transport can be explained by a small polaron hopping conduction mechanism. Hopping activation energies which varied slightly with dopant type in the range of 172–208 meV are obtained. The formation energies and charge ionization energies obtained for the dopants through our *ab initio* calculations are consistent with the differences in the experimental electrical properties of the doped systems. The obtained optical properties and band gap are also comparable to the experimentally obtained values. The complex dielectric functions of the doped and undoped NiO show the influence of the dopants on the optical properties of the NiO system. Experiments and computations both show that O-rich NiO films have high subgap absorption compared to NiO films, which is attributed to V_{Ni} defects induced *p-d* charge transitions. Our work demonstrates that among possible *p*-type dopants, Li is an efficient acceptor to achieve highly conducting *p*-type NiO with good mobility values especially at elevated temperatures and a >40% transmittance in the visible range.

ACKNOWLEDGMENTS

This work was supported by the General Research Fund of the Research Grants Council of Hong Kong SAR, China, under Project No. CityU 11267516 and CityU-SRG 7005106. Supercomputer and computational resources were provided by the Lehigh University (LU) High-Performance Computing Center. C.E.E acknowledges LU startup fund. C.P.L acknowledges the support of the startup fund from Shantou University under Project No. NTF18027, Guangdong Basic and Applied Basic Research Foundation (Project No. 2020A 1515010180), the Major Research Plan of the National Natural Science Foundation of China (Project No. 91950101), and the Optics and Photoelectronics Project (No. 2018KCXTD011). K.O.E was supported by the Hong Kong Ph.D. Fellowship No. HKPFS: PF16-02083, Research Grants Council, University Grants Committee, Hong Kong.

[1] K. H. L. Zhang, K. Xi, M. G. Blamire, and R. G. Egdell, *P*-type transparent conducting oxides, J. Phys.: Condens. Matter **28**, 383002 (2016).

[2] D. S. Ginley and C. Bright, Transparent conducting oxides, MRS Bull. **25**, 15 (2000).

[3] A. Stadler, Transparent conducting oxides—An up-to-date overview, Materials **5**, 661 (2012).

[4] B. A. D. Williamson, J. Buckeridge, J. Brown, S. Ansbro, R. G. Palgrave, and D. O. Scanlon, Engineering valence band dispersion for high mobility p-type semiconductors, Chem. Mater. **29**, 2402 (2017).

[5] G. Hautier, A. Miglio, G. Ceder, G.-M. Rignanese, and X. Gonze, Identification and design principles of low hole effective mass p-type transparent conducting oxides, Nat. Commun. **4**, 2292 (2013).

[6] Y. Zhang *et al.*, A self-powered broadband photodetector based on an n-Si(111)/p-NiO heterojunction with high photosensitivity and enhanced external quantum efficiency, J. Mater. Chem. C **5**, 12520 (2017).

[7] H. Kawazoe, H. Yanagi, K. Ueda, and H. Hosono, Transparent p-type conducting oxides: Design and fabrication of p-n heterojunctions, MRS Bull. **25**, 28 (2000).

[8] L. Xu *et al.*, Inverted perovskite solar cells employing doped NiO hole transport layers: A review, Nano Energy **63**, 103860 (2019).

[9] S. Sajid *et al.*, Breakthroughs in NiO_x-HTMs towards stable, low-cost and efficient perovskite solar cells, Nano Energy **51**, 408 (2018).

[10] G. Li *et al.*, Overcoming the limitations of sputtered nickel oxide for high-efficiency and large-area perovskite solar cells, Adv. Sci. **4**, 1700463 (2017).

[11] S. Lany, J. Osorio-Guillen, and Z. Alex, Origin of the doping asymmetry in oxides: Hole doping in NiO versus electron doping in ZnO, Phys. Rev. B **75**, 241203(R) (2007).

[12] J. Osorio-Guillén, S. Lany, and A. Zunger, Nonstoichiometry and hole doping in NiO, AIP Conf. Proc. **1199**, 128 (2010).

[13] W.-L. Jang, Y.-M. Lu, W.-S. Hwang, and W.-C. Chen, Electrical properties of Li-doped NiO films, J. Eur. Ceram. Soc. **30**, 503 (2010).

[14] W. Chen, F.-Z. Liu, X.-Y. Feng, A. B. Djurišić, W. K. Chan, and Z.-B. He, Cesium doped NiO_x as an efficient hole extraction layer for inverted planar perovskite solar cells, Adv. Energy Mater. **7**, 1700722 (2017).

[15] K. O. Egbo, M. Kong, C. P. Liu, and K. M. Yu, Room temperature sputtered Cu doped $NiO_{1+\delta}$: p-type conductivity, stability of electrical properties and p-n heterojunction, J. Alloys Compd. **835**, 155269 (2020).

[16] G. Natu, P. Hasin, Z. Huang, Z. Ji, M. He, and Y. Wu, Valence band-edge engineering of nickel oxide nanoparticles via cobalt doping for application in p-type dye-sensitized solar cells, ACS Appl. Mater. Interfaces **4**, 5922 (2012).

[17] S. Nandy, U. N. Maiti, C. K. Ghosh, and K. K. Chattopadhyay, Enhanced p-type conductivity and band gap narrowing in heavily Al doped NiO thin films deposited by RF magnetron sputtering, J. Phys.: Condens. Matter. **21**, 115804 (2009).

[18] R. Cao, H. X. Deng, and J. W. Luo, Design principles of p-type transparent conductive materials, ACS Appl. Mater. Interfaces **11**, 24837 (2019).

[19] D. A. G. Bruggeman, Berechnung verschiedener physikalischer Konstanten von heterogenen Substanzen. I. Dielektrizitätskonstanten und Leitfähigkeiten der Mischkörper aus isotropen Substanzen, Ann. Phys. **416**, 636 (1935).

[20] C. P. Liu *et al.*, Effects of Free Carriers on the Optical Properties of Doped CdO for Full-Spectrum Photovoltaics, Phys. Rev. Appl. **6**, 064018 (2016).

[21] P. Hohenberg and W. Kohn, Inhomogeneous electron gas, Phys. Rev. **136**, B864 (1964).

[22] W. Kohn and L. J. Sham, Self-consistent equations including exchange and correlation effects, Phys. Rev. **140**, A1133 (1965).

[23] J. P. Perdew, K. Burke, and M. Ernzerhof, Generalized Gradient Approximation Made Simple, Phys. Rev. Lett. **77**, 3865 (1996).

[24] G. Kresse and J. Furthmüller, Efficiency of ab-initio total energy calculations for metals and semiconductors using a plane-wave basis set, Comput. Mater. Sci. **6**, 15 (1996).

[25] O. Bengone, M. Alouani, P. Blöchl, and J. Hugel, Implementation of the projector augmented-wave LDA+U method: Application to the electronic structure of NiO, Phys. Rev. B **62**, 16392 (2000).

[26] C. E. E. Ekuma, V. I. I. Anisimov, J. Moreno, and M. Jarrell, Electronic structure and spectra of CuO, Eur. Phys. J. B **87**, 23 (2014).

[27] C. Freysoldt *et al.*, First-principles calculations for point defects in solids, Rev. Mod. Phys. **86**, 253 (2014).

[28] C. Rödl, F. Fuchs, J. Furthmüller, and F. Bechstedt, Quasiparticle band structures of the antiferromagnetic transition-metal oxides MnO, FeO, CoO, and NiO, Phys. Rev. B **79**, 235114 (2009).

[29] A. K. Cheetham and D. A. O. Hope, Magnetic ordering and exchange effects in the antiferromagnetic solid solutions $Mn_xNi_{1-x}O$, Phys. Rev. B **27**, 6964 (1983).

[30] M. Ain, A. Menelle, B. M. Wanklyn, and E. F. Bertaut, Magnetic structure of CuO by neutron diffraction with polarization analysis, J. Phys.: Condens. Matter **4**, 5327 (1992).

[31] B. X. Yang, T. R. Thurston, J. M. Tranquada, and G. Shirane, Magnetic neutron scattering study of single-crystal cupric oxide, Phys. Rev. B **39**, 4343 (1989).

[32] F. A. Kröger and H. J. Vink, Relations between the concentrations of imperfections in crystalline solids, Solid State Phys. **3**, 307 (1956).

[33] See Supplemental Material at http://link.aps.org/supplemental/10.1103/PhysRevMaterials.4.104603 for table of electrical resistivity as a function of dopant concentration, atomic projected density of states and Ni 2p high resolution XPS spectra.

[34] D. K. Schroder, *Semiconductor material and Device Characterization*, 3rd ed. (Wiley, 2006).

[35] B. Gunning, J. Lowder, M. Moseley, and W. Alan Doolittle, Negligible carrier freeze-out facilitated by impurity band conduction in highly p-type GaN, Appl. Phys. Lett. **101**, 082106 (2012).

[36] C. P. Liu, K. O. Egbo, C. Y. Ho, Y. Wang, C. K. Xu, and K. M. Yu, Wide-Gap $Zn_{1-x}Ni_xO$ Alloy: A Transparent p-Type Oxide, Phys. Rev. Appl. **13**, 024049 (2020).

[37] C. P. Liu, K. O. Egbo, C. Y. Ho, J. A. Zapien, W. Walukiewicz, and K. M. Yu, Stoichiometry Controlled Bipolar Conductivity in Nanocrystalline $Ni_xCd_{1-x}O_{1+\delta}$ Thin Films, Phys. Rev. Appl. **11**, 014019 (2019).

[38] N. Miller *et al.*, Hole transport and photoluminescence in Mg-doped InN, J. Appl. Phys. **107**, 113712 (2010).

[39] T. Dutta, P. Gupta, A. Gupta, and J. Narayan, Effect of Li doping in NiO thin films on its transparent and conducting properties and its application in heteroepitaxial *p-n* junctions, J. Appl. Phys. **108**, 083715 (2010).

[40] J. Y. Zhang, W. W. Li, R. L. Z. Hoye, J. L. Macmanus-driscoll, and M. Budde, Electronic and transport properties of Li-doped NiO epitaxial thin films, J. Mater. Chem. C **6**, 2275 (2018).

[41] S. C. Chen, T. Y. Kuo, Y. C. Lin, and H. C. Lin, Preparation and properties of *p*-type transparent conductive Cu-doped NiO films, Thin Solid Films **519**, 4944 (2011).

[42] R. Ishikawa *et al.*, Preparation of *p*-type NiO films by reactive sputtering and their application to CdTe solar cells, Jpn. J. Appl. Phys. **55**, 02BF04 (2016).

[43] H. Peng and S. Lany, Semiconducting transition-metal oxides based on *d*5 cations: Theory for MnO and Fe_2O_3, Phys. Rev. B **85**, 201202 (2012).

[44] H. Peng, P. F. Ndione, D. S. Ginley, A. Zakutayev, and S. Lany, Design of Semiconducting Tetrahedral $Mn_{1-x}Zn_xO$ Alloys and Their Application to Solar Water Splitting, Phys. Rev. X **5**, 021016 (2015).

[45] A. J. Bosman and H. J. van Daal, Small-polaron versus band conduction in some transition-metal oxides, Adv. Phys. **19**, 1 (1970).

[46] R. Karsthof, M. Grundmann, A. M. Anton, and F. Kremer, Polaronic interacceptor hopping transport in intrinsically doped nickel oxide, Phys. Rev. B **99**, 235201 (2019).

[47] L. Farrel, K. Fleischer, D. Caffrey, D. Mullarkey, E. Norton, and I. V. Shvets, Conduction mechanism in the epitaxial *p*-type transparent conducting oxide Cr_2O_3:Mg, Phys. Rev. B **91**, 125202 (2015).

[48] O. F. Schirmer, Holes bound as small polarons to acceptor defects in oxide materials: Why are their thermal ionization energies so high? J. Phys.: Condens. Matter **23**, 334218 (2011).

[49] C. P. Liu *et al.*, Room-temperature-synthesized high-mobility transparent amorphous CdO-Ga_2O_3 alloys with widely tunable electronic bands, ACS Appl. Mater. Interfaces **10**, 7239 (2018).